Atomic-interface strategy and N,O codoping enable WS_2 electrodes with ultrafast ion transport rate in sodium-ion batteries

Meisheng Han, Yongbiao Mu, Yuanyuan Cai, Lei Wei, Lin Zeng*, Tianshou Zhao*

Shenzhen Key Laboratory of Advanced Energy Storage, Southern University of Science and Technology, Shenzhen 518055, China

SUSTech Energy Institute for Carbon Neutrality, Southern University of Science and Technology, Shenzhen 518055, China

Department of Mechanical and Energy Engineering, Southern University of Science and Technology, Shenzhen 518055, China

*Corresponding Author.

E-mail address: zhaots@sustech.edu.cn (T.S. Zhao); zengl3@sustech.edu.cn (L. Zeng)

Experimental section

Synthesis of samples

The DMF and $(NH_4)_2WS_4$ was mixed in the self-made vessels in a distinct amount. Various WS_2/C examples were obtained by varying the proportion of DMF/$(NH_4)_2WS_4$ of 0.7/0.3 g (WS_2/C-I), 0.8/0.2 g (WS_2/C-II), and 0.9/0.1 g, (WS_2/C-III). After that, these vessels were sealed in an Ar-filled glove box and then transferred to a tube furnace, kept at 650 ^oC for 20 min in an Ar flow, and subsequently cooled naturally to obtain these samples. As a comparison, pure WS_2 was prepared by heating only 1 g $(NH_4)_2WS_4$ under the same conditions.

Characterizations

The microstructure and chemical composition were detected by SEM (Hitachi S-4700), TEM (FEI Talos F200x), Raman spectroscopy (Renishaw RM-1000), and XPS (TherW Scientific Escalab 250Xi), as well as EELS (FEI, Titan Themis G2), XRD (D/max-2500/PC, Rigaku), Elemental analysis (Perkinelmrr 2400 Series II) and TGA (Pyris I, PerkinElmer). The Brunauer-Emmett-Teller and Barrett-Joyner-Halenda (ASAP 2020, HD88) were employed to measure the surface area, and pore size distribution. The physical property measurement system (Quantum Design) was used to test the magnetic hysteresis curves. The TGA is tested in air atmosphere.

Electrochemical measurements

For half cells, the working electrodes were prepared by mixing active materials, acetylene black, and polyvinylidene fluoride (PVDF) with 8:1:1 in N-methyl

pyrrolidone solvent, which was then uniformly coated on the copper foil and dried at 85 ℃ for 12 h under vacuum. 2032 coin-type cells included working electrode, counter/reference electrode (sodium metal), and separator, as well as electrolyte, which were assembled in an Ar-filled glovebox. Whatman glass fiber was used as the separator. 1 M $NaClO_4$ in ethylene carbonate/dimethyl carbonate (volume ratio of 1:1) with 5% fluoroethylene-carbonate was used as electrolyte. The mass loading of active materials in each electrode slice was 1.2 mg cm^{-2}. Neware battery-test system (Shenzhen Neware Electronic co., China) was utilized to test the electrochemical performances of cells at current densities of 0.065-13 A g^{-1} from 0.01 and 3 V. A CHI 760D electrochemical workstation (Shanghai CH Instruments Co., China) was applied to measure CV and electrochemical impedance spectroscopy (EIS). CV was tested at a scanning rate of 0.1-1 mV s^{-1} from 0.01 to 3 V (vs. Na/Na^+). EIS was performed from 10^5 to 10^{-2} Hz with an amplitude of 5 mV.

For full cells, the cathode was prepared by mixing 80 wt% $Na_3V_2(PO_4)_2F_3$, 10 wt% acetylene black, and 10 wt% PVDF on Al foil. The mass ratio of anode and cathode was about 1:5. Before assembling full cells, the anode and cathode were electrochemically activated for three cycles at 0.065 A g^{-1}, respectively, to enhance their first CE. The voltage window was 1.0 to 3.5 V. All cells were tested at room temperature.

Computational method: We have employed the plane-wave code Vienna ab-initio simulation package (VASP) program to perform all the spin-polarized DFT calculations within the generalized gradient approximation using the

Perdew-Burke-Ernzerhof formulation. We have chosen the projected augmented wave potentials to describe the ionic cores and take valence electrons into account using a plane-wave basis set with a kinetic energy cutoff of 500 eV. Van der Waals (vdW) interactions are included with the DFT-D3 method of Grimme. Partial occupancies of the Kohn−Sham orbitals were allowed using the Gaussian smearing method and a width of 0.02 eV. The electronic energy was considered self-consistent when the energy change was smaller than 10^{-6} eV. To study the Na^+ diffusion kinetics in the WS_2, diffusion barriers were determined by using the climbing image nudged elastic band (CI-NEB) method.

Modeling description: The equilibrium lattice constants of [WS_2] unit cell was optimized, when using a 15×15×3 Monkhorst-Pack k-point grid for Brillouin zone sampling to be a=b= 3.18642, c=13.82469 Å. We set 10.8 spacings in the c-axis direction to represent the interlayer spacings of the catalyst. The 10.86% O atom and 8.96% N atom were located in WS_2 model to consider the effect of the co-doped O and N. The 6.34% O atom and 13.03% N atom were located in monolayer C model to consider the effect of the co-doped O and N. During structural optimizations of the models, a 3×3×1 gamma-point centered k-point grid for Brillouin zone was used. And all the atomic layers were allowed to fully relax.

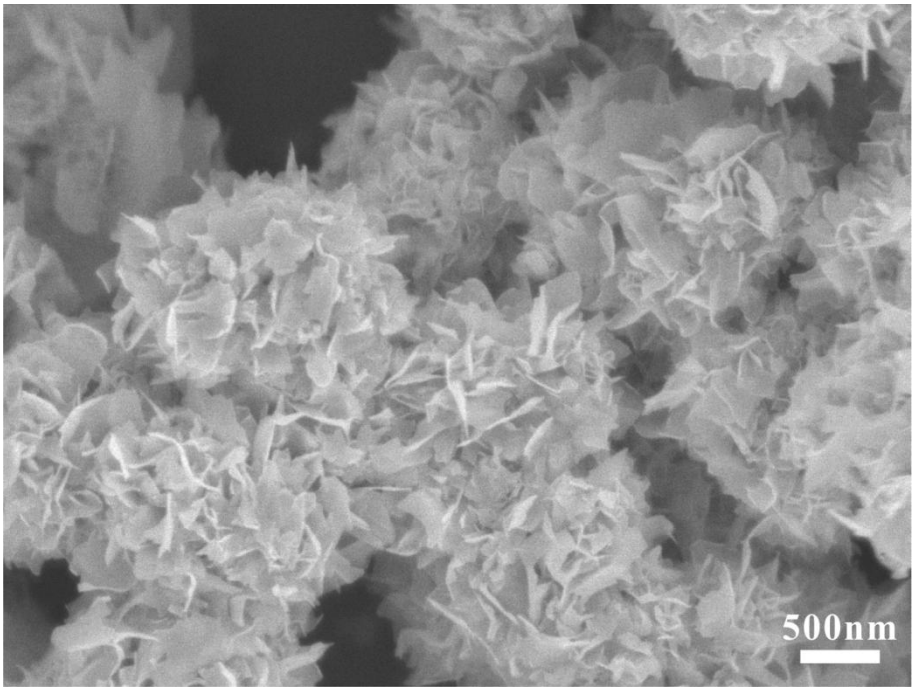

Figure S1. SEM image of WS_2/C-I.

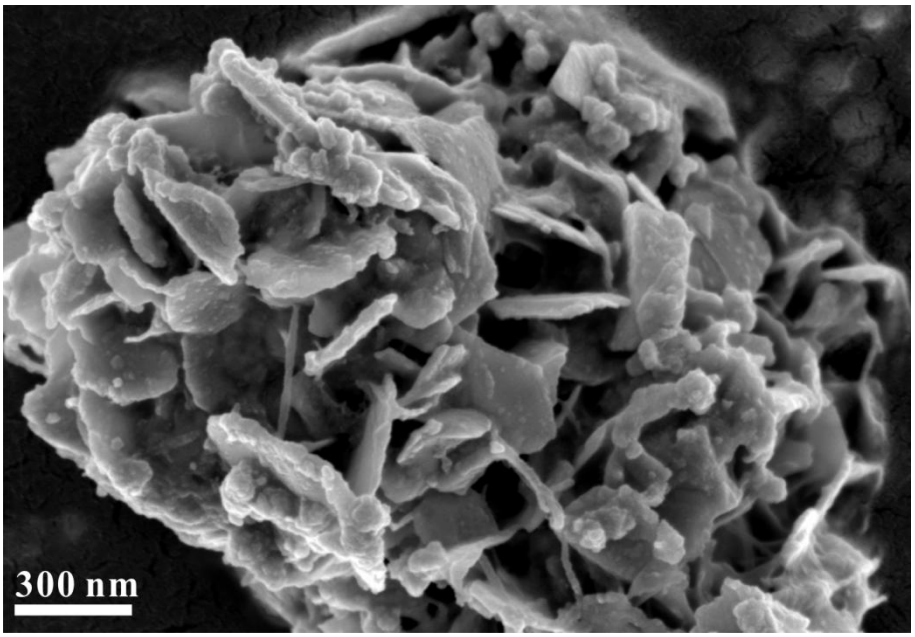

Figure S2. SEM image of WS_2/C-III.

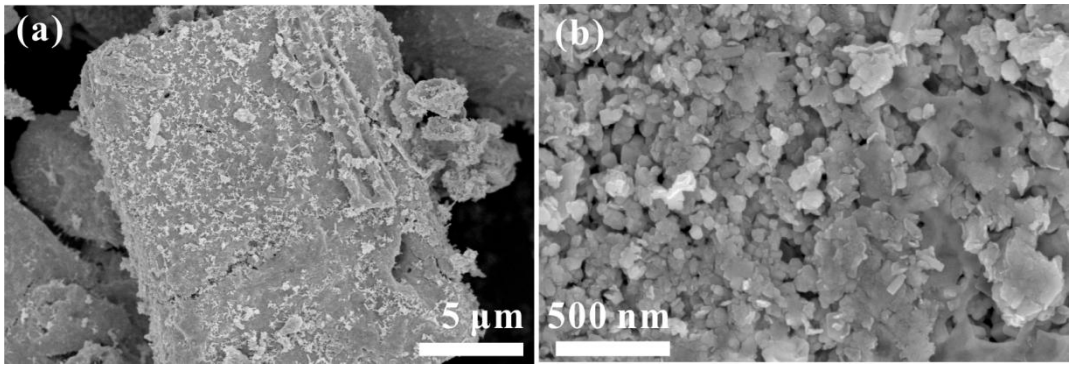

Figure S3. SEM images of WS_2.

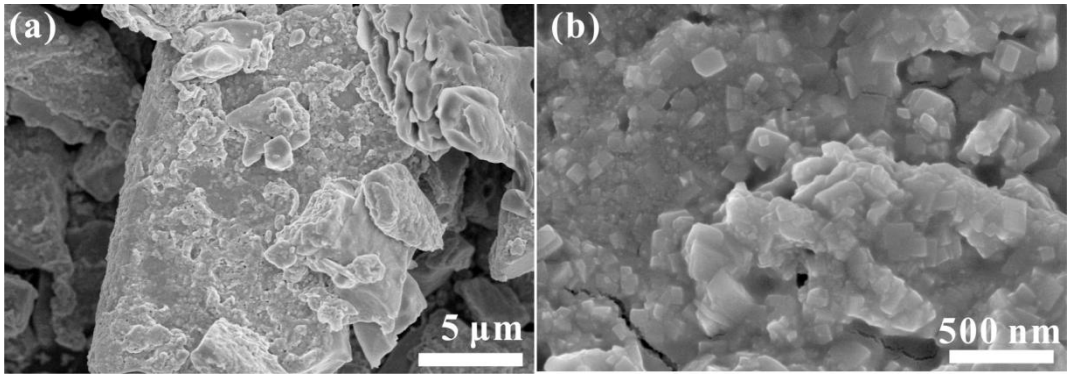

Figure S4. SEM images of $(NH_4)_2WS_4$.

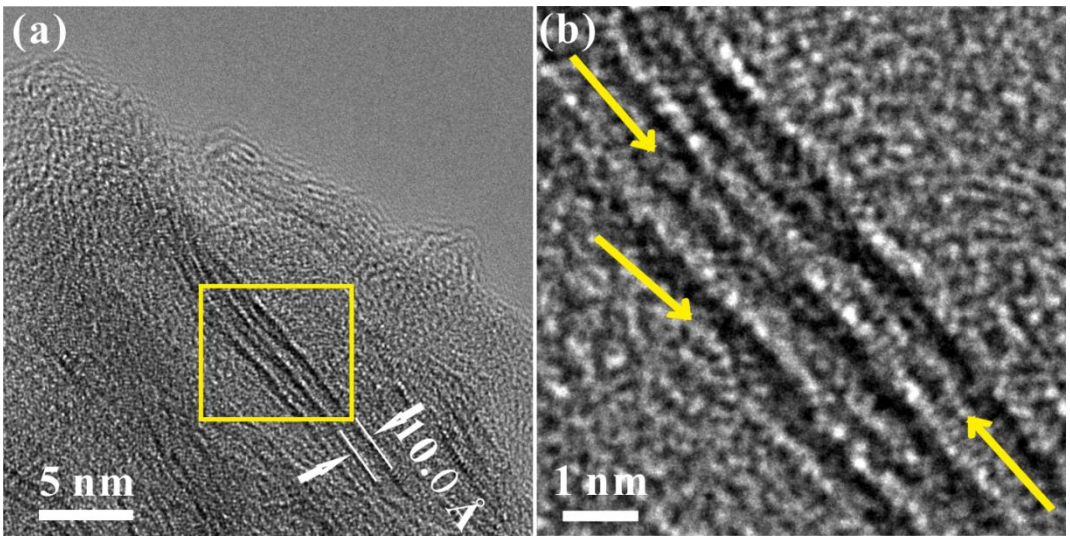

Figure S5. HRTEM images of WS_2/C-I

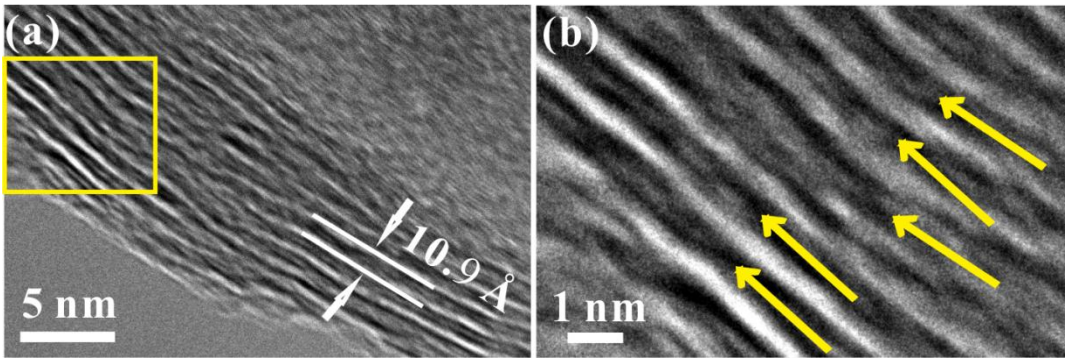

Figure S6. HRTEM images of WS_2/C-III.

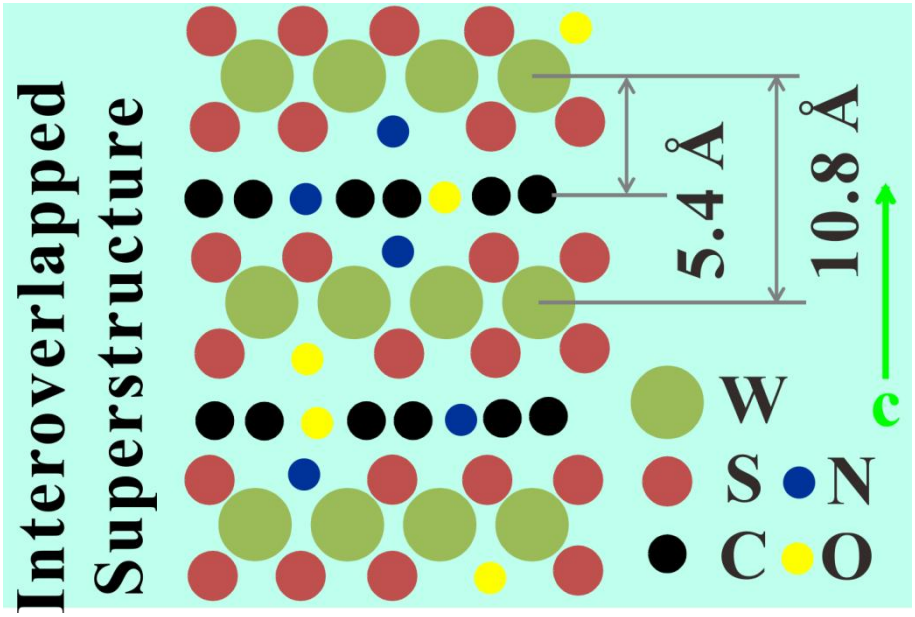

Figure S7. Schematic diagram of atomic structure of NO-WS_2-C

Table S1 Fitting results of XPS spectra of all the samples.

Samples	W (at%)	S (at%)	C (at%)	N (at%)	O (at%)
WS_2	32.89	64.90	0.89	0	1.32
WS_2/C-I	5.52	8.99	68.01	11.36	6.12
WS_2/C-II	4.52	6.31	69.23	12.51	7.43
WS_2/C-III	3.64	3.90	70.14	13.69	8.63

The atomic ratio of S and W elements in the WS_2, WS_2/C-I, WS_2/C-II and WS_2/C-III is 1.97, 1.63, 1.40 and 1.07, respectively.

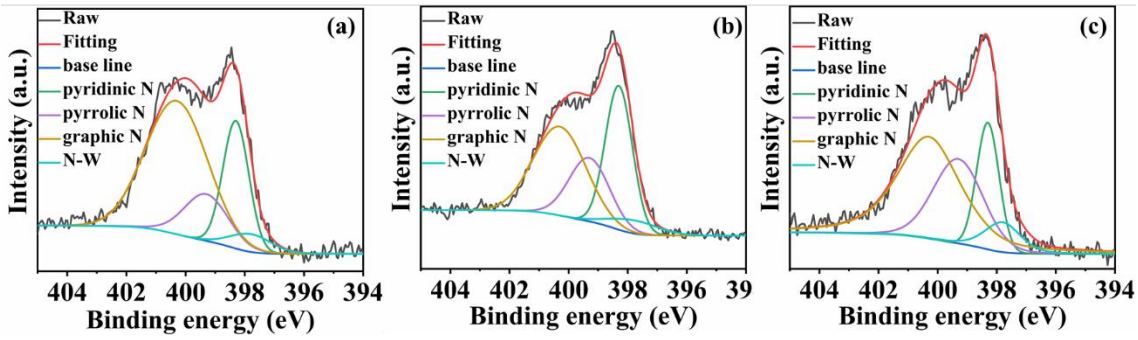

Figure S8. XPS spectra of N 1s of WS_2/C-I (a), WS_2/C-II (b), and WS_2/C-III (c).

Table S2 The percentages of various chemical bonds in N 1s.

Samples	N-W (%)	Pyridinic/pyrrolic/graphic N (%)
WS_2/C-I	5.49	94.51
WS_2/C-II	10.06	89.94
WS_2/C-III	14.11	85.89

The results are from Figure S8.

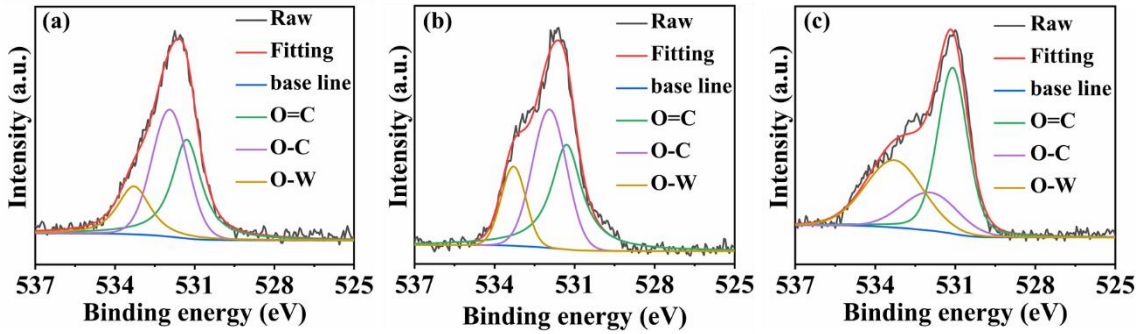

Figure S9. XPS spectra of O 1s of WS_2/C-I (a), WS_2/C-II (b), and WS_2/C-III (c).

Table S3 The percentages of various chemical bonds in O 1s.

Samples	O-W (%)	C-O/C=O (%)
WS_2/C-I	13.09	86.91
WS_2/C-II	20.78	79.22
WS_2/C-III	28.27	71.73

The results are from Figure S9.

Table S4 EC of the obtained samples

Samples	EC (S/cm)
WS_2	$2.1x10^{-4}$
WS_2/C-I	23.2
WS_2/C-II	37.4
WS_2/C-III	40.5

Electrical conductivity measurements

First, the obtained powders were added in a hollow cylinder mould with two electrodes on each ends, which were connected with a digital multimeter (Keithley 2001, USA) and followed by compressing powders into slices. During compressing, the electrical resistance was observed constantly. When the electrical resistance kept stable, the sample slices were obtained. Subsequently, the electrical conductivity of slices was measured using a four-probe tester (Probes Tech RTS-8, China)

The doping amount of N and O elements in the carbon materials was calculated by Pyridinic/pyrrolic/graphic N (%)*N (at%)/(C (at%)+Pyridinic/pyrrolic/graphic N (%)*N (at%)+C-O/C=O (%)*O (at%))*100% and C-O/C=O (%)*O (at%)/(C (at%)+Pyridinic/pyrrolic/graphic N (%)*N (at%)+C-O/C=O (%)*O (at%))*100%, respectively. The specific doping amount was represented in **Table S5**.

Table S5 The doping amount of N and O elements in the carbon materials

Samples	N (at%)	O (at%)
WS_2/C-I	12.83	5.92
WS_2/C-II	13.03	6.34
WS_2/C-III	13.34	6.48

The doping amount of N and O elements in the WS_2 materials should be calculated by N-W (%)*N (at%)/[W (at%)+S (at%)+N-W (%)*N (at%)+O-W (%)*O (at%)]*100% and O-W (%)*O (at%)/[W (at%)+S (at%)+N-W (%)*N (at%)+O-W (%)*O (at%)]*100%, respectively. The specific doping amount is represented in **Table S6**.

Table S6 The doping amount of N and O elements in the WS_2 materials

Samples	N (at%)	O (at%)
WS_2/C-I	4.05	5.98
WS_2/C-II	8.96	10.86
WS_2/C-III	14.21	16.79

Table S7 The elemental analysis results of the obtained samples.

Samples	C (wt%)	N (wt%)	O (wt%)	WS_2 (wt%)
WS_2/C-I	11.25	3.31	1.88	83.56
WS_2/C-II	18.43	5.42	3.97	72.18
WS_2/C-III	28.99	7.58	4.64	58.79

The C, N, and O contents in the composites were measured using O/N/H and C/S elemental analyzers. The content of WS_2 was calculated as a difference to 100 wt%.

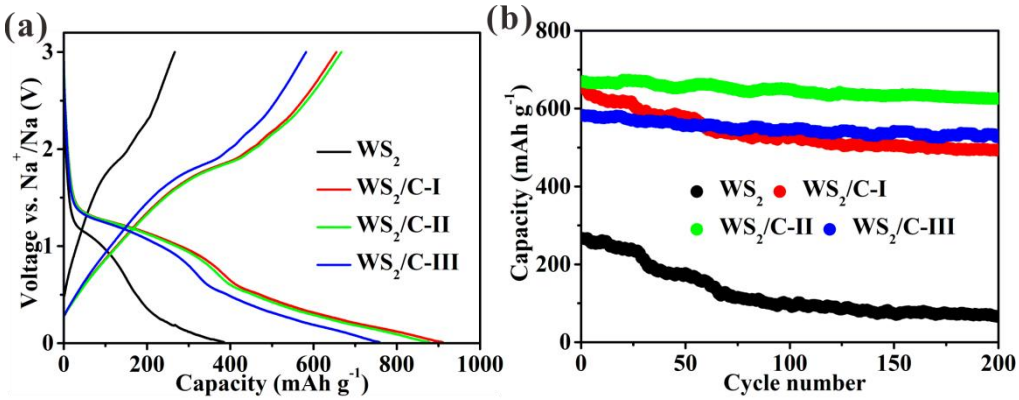

Figure S10 (a) First charge and discharge curves, and (b) cycling performances at 0.065 A g^{-1} of the as-prepared samples.

Table S8 The charge capacity and charge capacity retention after 200 cycles of the obtained samples.

Samples	First capacity (mAh g^{-1})	Final capacity (mAh g^{-1})	Capacity retention (%)
WS_2	266.2	65.7	24.7
WS_2/C-I	655.3	494.5	75.5
WS_2/C-II	669.2	661.8	98.9
WS_2/C-III	582.8	554.6	95.2

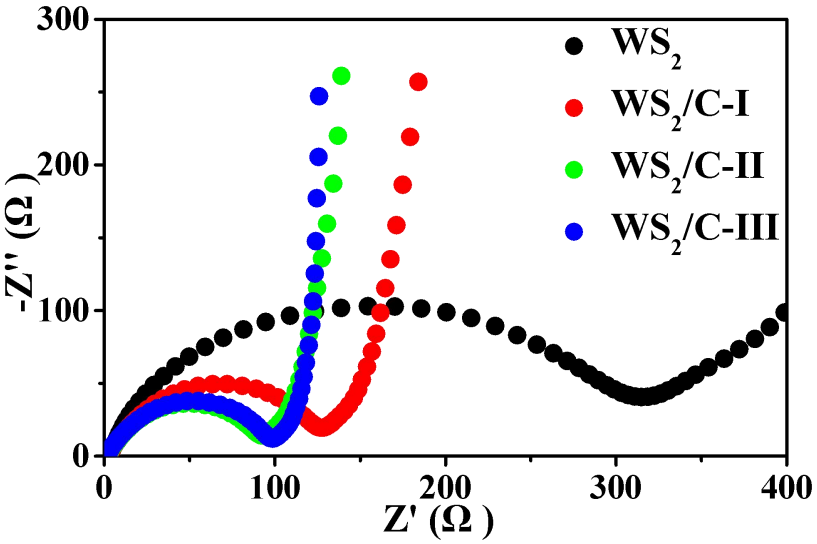

Figure S11. Nyquist plots of the obtained samples before cycling.

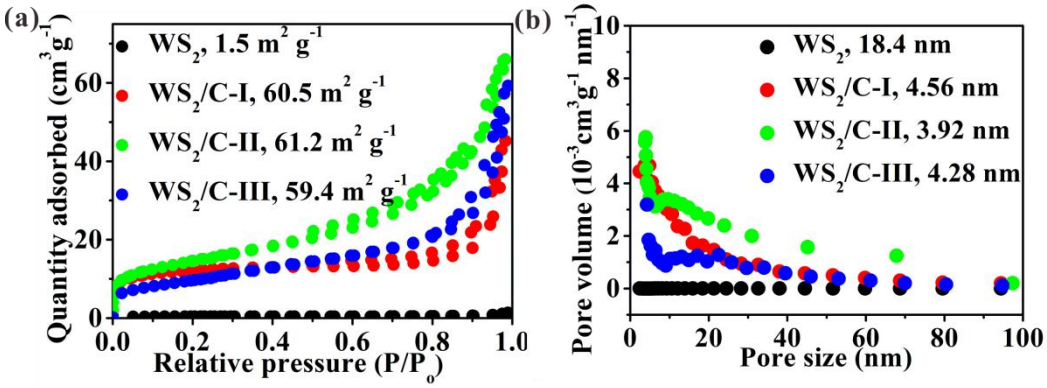

Figure S12. (a) Nitrogen adsorption/desorption isotherms and (b) pore size distribution of the obtained samples.

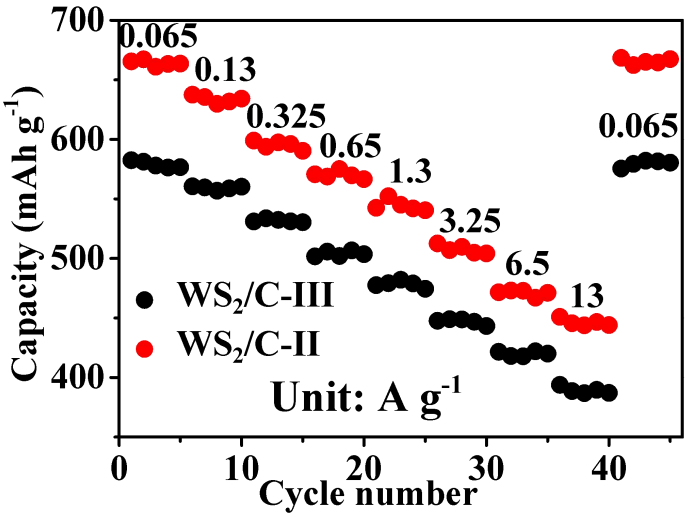

Figure S13. The comparison of rate capability between WS_2/C-II and WS_2/C-III electrodes.

The capacity of WS_2/C-II is 665.5 and 450.8 mAh g^{-1} at 0.065 and 13 A g^{-1}, respectively. The capacity obtained at 13 A g^{-1} maintains 67.7% of the capacity obtained at 0.065 A g^{-1}. The capacity of WS_2/C-III is 582.5 and 389.6 mAh g^{-1} at 0.065 and 13 A g^{-1}, respectively. The capacity obtained at 13 A g^{-1} maintains 66.9% of the capacity obtained at 0.065 A g^{-1}. The results indicate that the WS_2/C-II has higher capacity and corresponding higher capacity retention at high rate test than that of the WS_2/C-III.

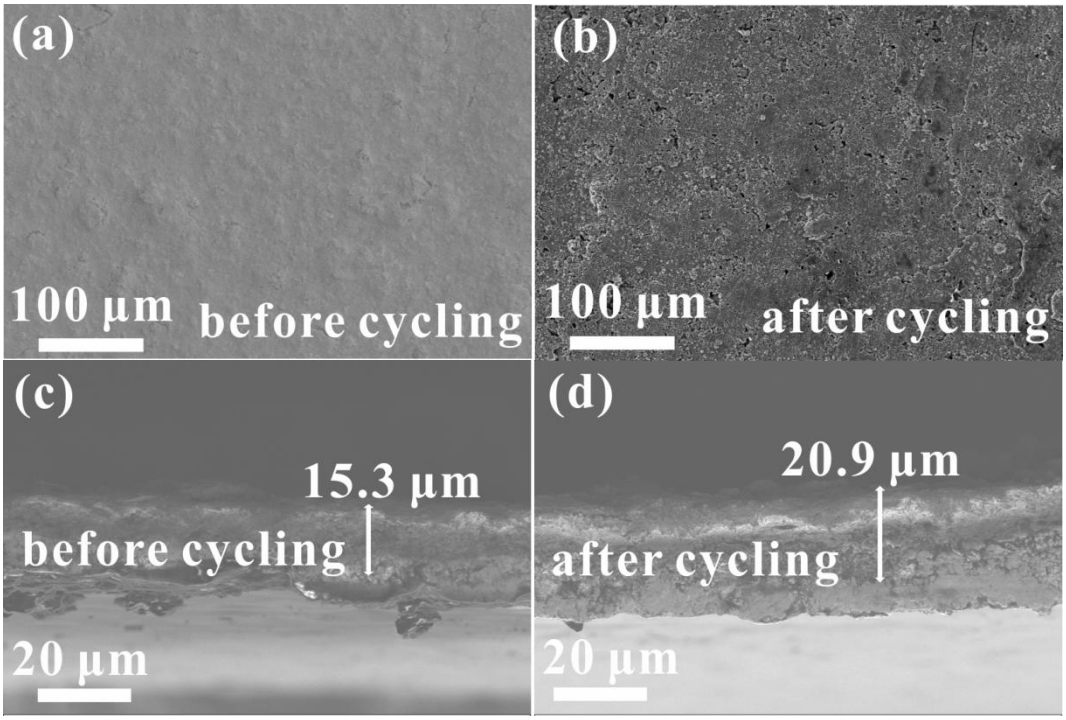

Figure S14 SEM images of WS_2/C-II electrodes before and after 200 cycling.

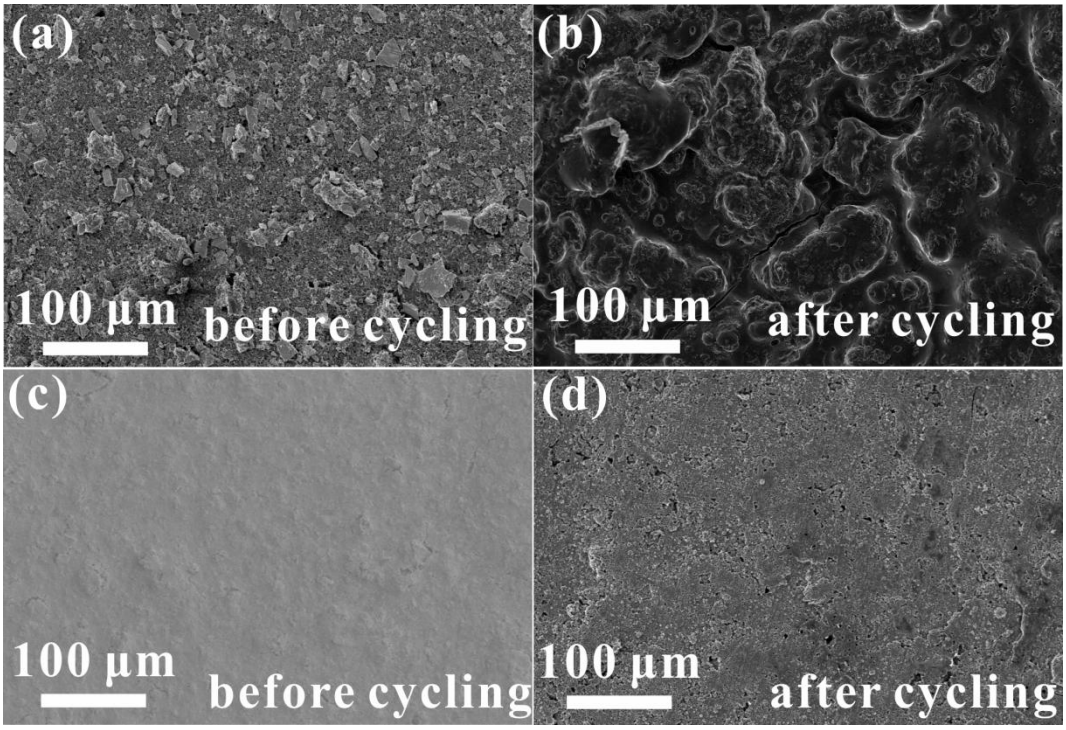

Figure S15. Surface SEM images of pure WS_2 (a,b) and WS_2/C-II (c,d) electrodes before and after cycling.

Table S9. Comparison of the initial CE of the WS_2 or nanocomposites of WS_2 and carbon materials as anodes for SIBs with our work.

Samples	Initial CE	Reference
WS_2/C-II	**76.2%**	**This work**
H-WS_2@NC	67.7%	Adv. Funct. Mater. 2020, 30, 1907677
WS_2 nanoflakes	55.8%	Sustain. Energy Fuels 2019, 3, 1239.
WS_2/rGO	52.1%	Carbon 2019, 142, 697.
NGQDs-WS_2/3DCF	55.2%	J. Mater. Chem. A 2018, 6, 10813.
WS_2/NC	62.5%	Front. Chem. 2018, 6, 236.
WS_2/CNT-rGO	33.9%	Adv. Energy Mater. 2016, 6, 1601057.
WS_2 nanowires	67.6%	Chem. Eur. J. 2015, 21, 11878.
WS_2-3D RGO	56%	Nanoscale 2015, 7, 3965

Table S10 The specific references about capacity comparison of WS_2-based SIB anodes after long cycling under high current denisities from Figure 4h in the manuscript. C_C-charge capacity (mAh g^{-1}) after cycling, J-current density (A g^{-1}), N_C-cycle number.

Samples	C_C	J	N_C	References
WS_2/C-II	**518.2**	**1.3**	**3000**	**This work**
WS_2/C-II	**378.3**	**6.5**	**3000**	**This work**
FeS_2/WS_2-CNFs	307.6	4	1000	Chem. Eng. J. 427 (2022) 131002
H-WS_2@NC	375	1	1000	Adv. Funct. Mater. 30 (2020) 1907677
WS_2/CFC@C-P	297	2	500	Chem. Eng. J. 411 (2021) 128554
1T $W_{0.9}Mo_{0.1}S_2$	411	0.1	180	J. Energy Chemistry 66 (2022) 356-365
WS_2@NC	150	5	500	J. Mater. Chem. A, 5 (2017) 10406-10415
NGQDs-WS_2/3DCF	392.1	0.2	1000	J. Mater. Chem. A, 6 (2018) 10813-10824
HB WS_2@CNFs	343	2	300	Small, 16 (2020) 2000695
WS_2 Nanowires	370	1	1400	Chem. Eur. J. 21 (2015) 11878-11884

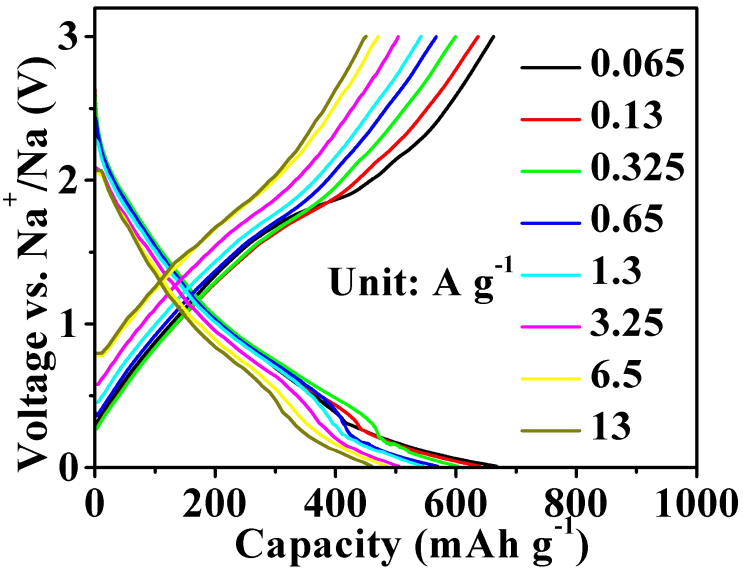

Figure S16. Charge/discharge curves at differenct current densities of WS_2/C-II

Table S11 The specific references about comparison of rate performances of WS_2-based SIB anodes from Figure 4i in the manuscript.

Samples	References
WS_2/C-II	**This work**
FeS_2/WS_2-CNFs	Chem. Eng. J. 427 (2022) 131002
H-WS_2@NC	Adv. Funct. Mater. 30 (2020) 1907677
WS_2/CFC@C-P	Chem. Eng. J. 411 (2021) 128554
1T $W_{0.9}Mo_{0.1}S_2$	J. Energy Chemistry 66 (2022) 356-365
WS_2/CNT-rGO Aerogel	Adv. Energy Mater. 6 (2016) 1601057
NGQDs-WS_2/3DCF	J. Mater. Chem. A, 6 (2018) 10813–10824
HB WS_2@CNFs	Small, 16 (2020) 2000695

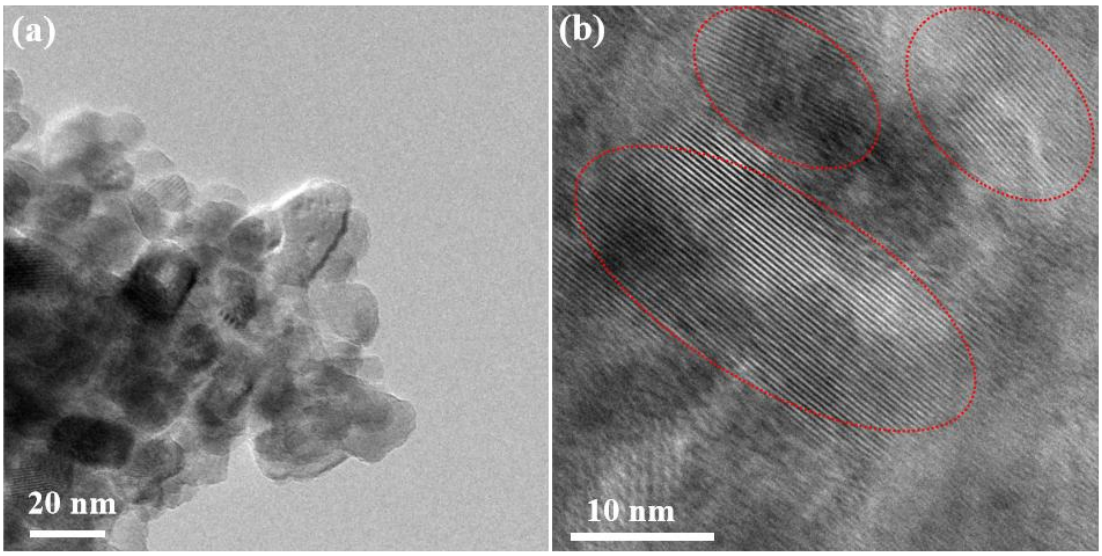

Figure S17. TEM images of pure WS_2 electrode after discharging to 0.01 V.

Na-Ion Concentration Calculation

At first, the unit cell volume of WS_2 is calculated to be "a (3.15 Å) × b (3.15 Å) × c (12.27 Å) × sin120° = 105.44 × 10^{-24} cm^3", thus 1 cm^3 includes 1/105.44 × 10^{-24} = 9.48 × 10^{21} unit cells. The charge capacities of WS_2/C-I, WS_2/C-II, and WS_2/C-III can reach 655.3, 669.2, and 582.8 mAh g^{-1}, respectively during the initial cycling, corresponding to 1.52, 1.55, and 1.35 Na^+ insertion into WS_2 per formula unit to form the $Na_{1.52}WS_2$, $Na_{1.55}WS_2$, and $Na_{1.35}WS_2$, respectively. In addition, every WS_2 unit cell includes two molecules, and each molecule includes 1.52, 1.55, and 1.35 Na-ions, 1 cm^3 contains 9.48 × 10^{21}/(6.02 × 10^{23}) × 2 × 1.55 = 4.79 × 10^{-2}, 4.88 × 10^{-2}, and 4.25× 10^{-2} mol Na-ions for WS_2/C-I, WS_2/C-II, and WS_2/C-III, respectively. As a result, the Na-ion concentration in the WS_2/C-I, WS_2/C-II, and WS_2/C-III electrode is about 4.79 × 10^{-2}, 4.88 × 10^{-2}, and 4.25× 10^{-2} mol cm^{-3}, respectively.

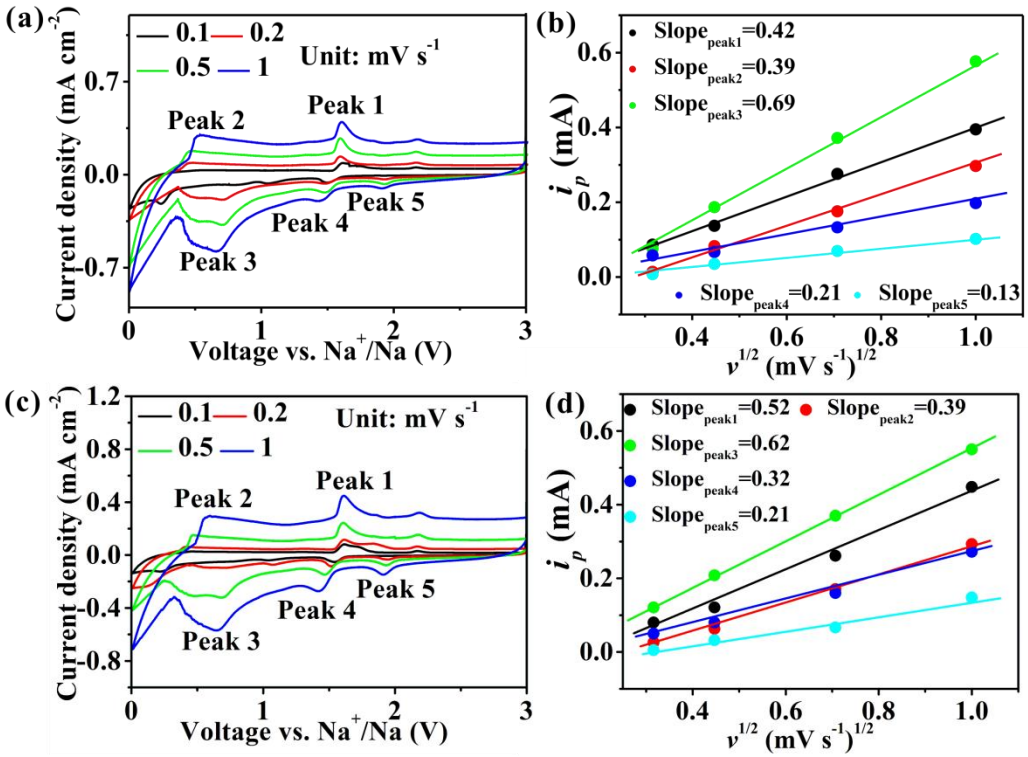

Figure S18. Kinetic analysis of WS_2/C-I (a,b) and WS_2/C-III (c,d). (a,c) CV curves from 0.1 to 1 mV s^{-1}; (b,d) Linear relationship between i_p and $v^{1/2}$.

Table S12 The specific references about comparison of D_{Na+} ($cm^2\ s^{-1}$) values of our WS_2/C-II and recently reported anode materials for SIBs.

Samples	D_{Na+}	References
WS_2/C-II	**1.50×10^{-9}**	**This work**
bare WS_2	2.42×10^{-15}	Adv. Funct. Mater. 30 (2020) 1907677
S-WS_2@NC	5.29×10^{-14}	Adv. Funct. Mater. 30 (2020) 1907677
H-WS_2@NC	8.23×10^{-13}	Adv. Funct. Mater. 30 (2020) 1907677
Vertical WS_2/C	2.14×10^{-10}	J. Mater. Chem. A 7 (2019) 25985-25992
FeS_2/WS_2-CNFs	1.12×10^{-14}	Chem. Eng. J. 427 (2022) 131002
WS_2/CFC@C-P	5.25×10^{-12}	Chem. Eng. J. 411 (2021) 128554
WS_2/CFC	5.25×10^{-13}	Chem. Eng. J. 411 (2021) 128554
1T $W_{0.9}Mo_{0.1}S_2$	7×10^{-10}	J. Energy Chemistry 66 (2022) 356-365

Table S13. The comparison of electrochemical performances for the full cells.

Samples	Current density	Specific capacity (mAh g^{-1})	The capacity is calculated based on	References
WS_2/C-II	**1.95 A g^{-1}**	**429.6 after 300 cycles**	**anode**	**This work**
VA/LT-WS_2/C	0.05 A g^{-1}	133 after 50 cycles	anode	Energy Storage Mater. 26 (2020) 534-542
WS_{2-X}/ZnS@C	1 A g^{-1}	89 after 500 cycles	anode	Adv. Mater. 32 (2020) 2005802
H-WS_2@NC	0.5 A g^{-1}	296 after 200 cycles	anode	Adv. Funct. Mater. 30 (2020) 1907677
1T $W_{0.9}Mo_{0.1}S_2$	1 A g^{-1}	143 after 50 cycles	anode	J. Energy Chemistry 66 (2022) 356-365